Local Scour for Side Slopes Piers with Upstream Lenticular Nose

Mohamed T. Shamaa

Abstract— Reducing local scour at bridge piers is very important to insure stability of bridges crossing watercourses. Laboratory experiments in this paper are presented to reduce maximum scour at side slope piers with upstream lenticular nose and side slope piers with upstream lenticular nose and upstream curved face. Experiments were implemented in a rectangular laboratory flume has 15 cm sand layer as bed material using clear water condition. The effects of Froude number, slope and normalized arc height on scour depth at piers nose are illustrated. Results analysis indicates that piers with sharp curved nose and upstream curved face gave the maximum reduction of scour depth at piers nose in this study. Empirical relations are formulated to forecast maximum scour depth at noses of bridges piers.

Key words: Bridges piers, side slope piers, scour depth, piers with upstream lenticular nose.

1 Introduction

SCOUR at bridge piers along watercourses may cause breakdown of bridges. Scour mechanism leads to erosion of sediments around submerged supporting elements in flow field and threaten the structural safety.

There are three types of scour may occur at bridge piers referred to as general scour, local scour and contraction scour. Several investigators indicate that local scour is the most critical type of scour, [6].

Interaction between piers and flow field leads to vertical stagnation flow and two boundary layers flows along the upstream pier perimeter. Vertical stagnation flow produces upward flow and downward flow jet at nose of pier. This downward flow component is directed to bed causing erosion.

The boundary layers resulting from interaction between pier and flow form a wake flow zone filled with vortices [3]. Shape of pier is a vital agent in the formation and the strength of the vortex system that consists of horseshoe vortex, wake vortex system, and surface roller (bow wave vortex), [2], [16], [17]. Horseshoe vortex developed at excavated scour hole by downward flow due to flow separation. Horseshow vortex transports the removed particles away downstream the pier. The horseshoe vortex strength diminishes as the scour depth increases.

Several investigators performed experiments and observed that the reduction of maximum depth of scour vastly dependent on shape factor [2], [3], [15]. Al-Shukur A.K. and Obeid Z. H. [2] concluded that rectangular shape of pier has higher scour depth compared with other shapes due to maximum exposed area. Also, they concluded that streamline pier produce smaller scour depth due to minimum exposed area. Experimental study in [1] clarified the scour development around semi-conical piers and explained the influence of their side slopes on scour depth. Results revealed that piers with side slopes reduce scour depth around pier. Piers with big side slope angle and circular cross section decreased scour depth upstream and downstream pier by 36% and 53% respectively compared with cylinder piers.

El- Alfy, K.S., Shamaa, M.T et al. used piers with side slope angle as scour countermeasure and compared the results with vertical cylindrical pier. Also, they used devices incorporated with leading edge of these piers. Under the condition of steady clear-water scour with 4 hours duration test, the results indicated decrease in depth and volume of scour for piers with different side slope angles compared with cylindrical pier [7]. The results also revealed that increasing the side slope angle of pier decrease depth and Volume of scour. According to devices incorporated with the leading edge of piers have side slope angle; the modified pier with upstream curved face gave the smallest volume of scour and smallest depth of scour in their study, [7], [8].

This study is concern on shapes of piers by decreasing the projected area, downward flow component and accordingly horse shoe vortex strength. Side slopes piers with upstream lenticular nose and side slopes piers with upstream lenticular nose modified using upstream curved face were used to decrease scour depth at pier's nose. Empirical relations are presented in this research to predict the scour depth at pier's nose for the studied types of piers.

2 Dimensional Analyses

There are four groups of variables influence local scour at piers. The first group related to fluid flow contains kinematic viscosity (υ), gravitational acceleration (g) and density of water (ρ), Flow intensity, flow depth (y), mean velocity (V), shear velocity and critical mean flow velocity (Vc). The second group related to fluid flow contains sediment density (ρ_s), the median size of particles d_{50}, geometric standard deviation of particles

- *Mohamed T. Shamaa is Associate Prof. Irrigation & Hydraulics Dept., Faculty of Engineering, Mansoura University, Egypt. E-mail: tarekshamaa@yahoo.com*

size distribution (σ_g). Third group related to pier contains pier size, pier length (l), pier width (b), side slope angle of pier (α), arc height curvature of upstream face of pier and attack angle (θ). The fourth group is test duration time T, [11].

Dimensional analysis provides a powerful method in formulating relations. Dimensional analysis is made herein for variables that affect the local scour mechanism by using Buckingham π-theorem.

The dependent scour depth d_s is expressed as function of the independent variables as:

$$d_S = f(V, Vc, \upsilon, g, \rho, y, \rho s, d_{50}, \sigma_g, l, b, Rc, a, \theta, T) \quad (1)$$

Using the repeating variables (ρ, V, y) in Buckingham's π theorem, dimensionless relationship can be represented as:

$$\frac{d_s}{y} = f\left(\frac{V}{V_C}, \frac{V^2}{gy}, \frac{b}{y}, \frac{Vy}{\upsilon}, \frac{d_{50}}{y}, \frac{VT}{y}, \frac{l}{y}, \frac{R_c}{y}, \sigma_g, SF, \frac{\rho_s}{\rho}, \theta, \alpha\right) \quad (2)$$

Equation (2) can be simplified and arranged as follow:

$$\frac{d_s}{y} = f\left(\frac{V}{V_C}, \frac{V^2}{gy}, \frac{VT}{b}, \frac{Vd_{50}}{\upsilon}, \frac{l}{y}, \frac{R_c}{y}, \sigma_g, SF, \frac{\rho_s}{\rho}, \theta, \alpha\right) \quad (3)$$

Reynolds number of Particle (Vd_{50}/ν) can be ignored for fully turbulent flow [10]. Also, (σ_g) can be ignored where bed material are not changed [10]. The densities of sediment and fluid are constant, so (ρ_s/ρ) can be ignored [11]. Attack Angle is kept constant equal 0°and, so θ is ignored. Factor (l/y) can be ignored where pier length (l) and water depth y are kept constant. Shape factor (S_F) is ignored where the variation in pier shapes is related to variation in side slope angle and not due to use piers of different shapes with similar perpendicular width relative to flow direction. If the duration of flow is long enough and the depth of equilibrium scour is reached, (VT/b) can be ignored [13]. Due to armoring effect, (V_a) replace (V_c) in Eq.(3).

Simplification of equation (3) leads to:

$$\frac{d_s}{y} = f\left(\frac{V}{V_a}, \frac{V}{\sqrt{gy}}, \frac{R_c}{y}, \alpha\right) \quad (4)$$

For side slopes piers with lenticular nose, $\frac{R_c}{y}$ is ignored and equation (4) becomes:

$$\frac{d_s}{y} = f\left(\frac{V}{V_a}, \frac{V}{\sqrt{gy}}, \alpha\right) \quad (5)$$

For side slopes piers with lenticular nose modified with upstream curved face, side slope angle is kept constant, so equation (4) becomes:

$$\frac{d_s}{y} = f\left(\frac{V}{V_a}, \frac{V}{\sqrt{gy}}, \frac{R_c}{y}\right) \quad (6)$$

Scour phenomena were studied at side slopes piers with lenticular nose and side slopes piers with lenticular nose modified with upstream curved face. Empirical relations were derived using nonlinear regression in statistical program SPSS for estimating the maximum dimensionless scour depth at pier nose. Statistical performance indicators were used to test the accuracy of these relations. These indicators are coefficient of determination (R^2), mean absolute error (MAE), mean absolute per-cent errors ($MAPE$) and root mean square error ($RMSE$). These statistical indicators are defined as follows, [9]:

$$MAE = \frac{1}{N}\sum_{i=1}^{N}\left|\left(\frac{ds}{y}\right)_{measured} - \left(\frac{ds}{y}\right)_{estimated}\right| \quad (7)$$

$$MAPE = \frac{100}{N}\sum_{i=1}^{N}\frac{\left|\left(\frac{ds}{y}\right)_{measured} - \left(\frac{ds}{y}\right)_{estimated}\right|}{\left(\frac{ds}{y}\right)_{measured}} \quad (8)$$

$$RMSE = \sqrt{\frac{\sum_{i=1}^{N}\left|\left(\frac{ds}{y}\right)_{measured} - \left(\frac{ds}{y}\right)_{estimated}\right|}{N}} \quad (9)$$

3 Experimental Set Up

Experiments were performed in a rectangular flume at Laboratory of Hydraulics and Irrigation, Faculty of Engineering, Mansoura University, Egypt. The flume is 40 cm depth, 6.8m length, and 74 cm width. Centrifugal pumps convey water to the flume from underground water tank through two water tanks. A tail gate is attached at channel end to control water. Discharge is determined by a rectangular weir fixed at entry section of approaching basin. Inlet mesh box filled with gravel is fitted downstream of approaching basin to decrease turbulence of water. The flume has moving point gauge has vertical scale and Vernier with accuracy of ± 0.1mm to measure vertical depths. Sand trap is located at end section of flume to prevent sand deposition in underground tank. General view of the channel is shown in Fig. (1).

4 Material of Bed

The channel bed is covered with sand layer of height 15 cm and d_{50}=0.63 mm. Geometric standard deviation of particle size distribution ratio σ_g = 2.34 mm. According to value of (σ_g), sand is considered non-uniform. Sand bed was leveled before the run and compacted with wood plate has the same width of flume. After that the pier was positioned cautiously in test section. The flume was then filled slowly after closing of downstream tailgate.

Components of flume that shown in Figure (1) are:

(1) Centrifugal pumps	(2) First head tank
(3) Second head tank	(4) rectangular weir
(5) Approach basin	(6) inlet mesh box
(7) Sand bed	(8) Wood bracing
(9) Pier model	(10) Sand trap
(11) Tail gate	(12) Collecting tank
(13) Graduated tank	(14) Underground tank
(15) Side walk	(16) Rails for point gauge

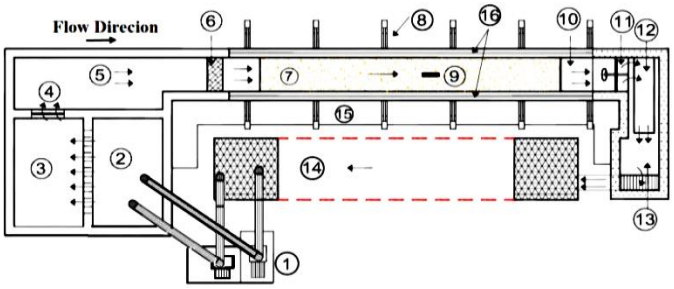

Fig. (1) Plan of experimental flume.

Experimental run were performed at beginning of study, to determine the suitable runs duration. The initial test were carried out for 6 hours with discharge Q = 26.124 lit/sec and

Froude number Fr = 0.3564. Measurements of scour depth at pier nose were recorded every 20 minutes and illustrated in Fig. (2). Scour depth does not significantly alter with time after four hours. At six hours, the depth of scour does not change in comparison with its counterpart at five hours. Error in measuring scour depth at four hours relative to scour depth at six hours is about 1 %. Bozkus and Cesme 2010, [5], [8], [9], indicate that change rate of scour depth is negligibly small after four hours. Also, [12]and [18] mention that most of scour occurs during first three or four hour of test. Thus, four hours were selected as test duration in this study.

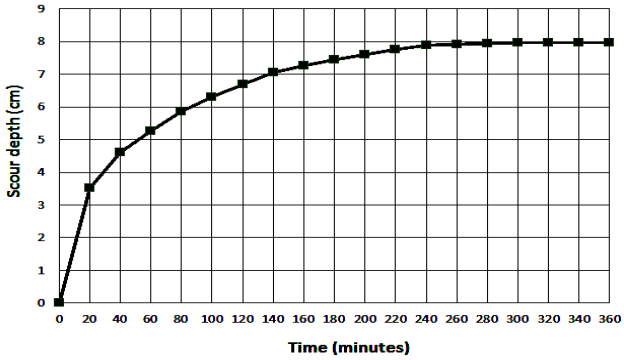

Fig. (2) Time development of scour depth for side slopes pier with Fr = 0.3564

5 PIERS

Wood piers painted with varnish and white oil paint to avoid water penetration. After that, sand was leveled and pier was placed with orientation 0° degree to flow direction in flume center. Used pier shapes are illustrated in Fig. (3). Also, dimension of piers used in this study are displayed in TABLE 1 and TABLE 2. The length (l) of piers was chosen based on ratio (l/b = 3), where b = (b_1+b_2)/2 is the mean width of pier. Lengths of piers have no influence on local scour since an attack angle for all experiments are kept constant.

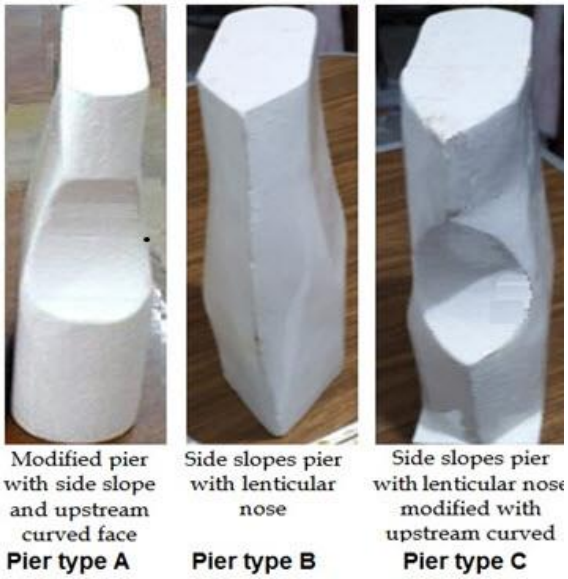

Fig. (3) Used pier shapes in study

Based on previous studies:
$\frac{\text{pier diameter (D)}}{\text{flume width } (B)} < 0.16$ to avoid influence of potential flow blockage on local scour at pier [14]. This criterion is achieved in this study where $\frac{\text{pier width } (b)}{\text{flume width } (B)} < 0.1$.

Also, $\frac{\text{pier diameter at bed level}}{\text{median sediment size of possible coarsest armor} d50a} > 25$ to avoid the sediment size effect on scour depth [1], [5]. This criterion is achieved in this study where $\frac{b2}{d50a} = 49.6$. Width of pier at bed level b_2 in this study for all used piers is kept constant equals 6.5 cm and $d50a$ equals (d_{max})/1.8 = 1.3111mm, where d_{max} is the maximum particle size equals 2.36 mm.

Plan of side slopes pier with lenticular nose and side slopes pier with lenticular nose and upstream curved face is illustrate in Fig. (4). Side view of side slopes pier with lenticular nose is illustrated in Fig. (5). Elevation of side slopes pier with lenticular nose and upstream curved face is illustrate in Fig. (6).

The arc height of curvature Rc in Fig.(6) is suggested to equal (D_2-D_1), [8]. The curvature begins from water surface level to bed level through nose of pier. This curvature exists in upstream face of pier and not affects the supporting element. In Fig. (6) the radius of circle is computed as [7], [8]:

$$r = \frac{y^2}{8\,R_c} + \frac{R_c}{2} \qquad (10)$$

where, y is water depth.

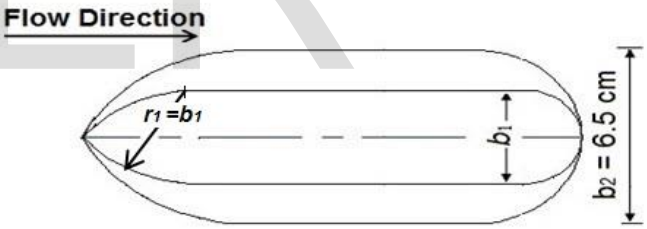

Fig. (4) Plan of side slopes pier with lenticular nose and side slopes pier with lenticular nose and upstream curved face.

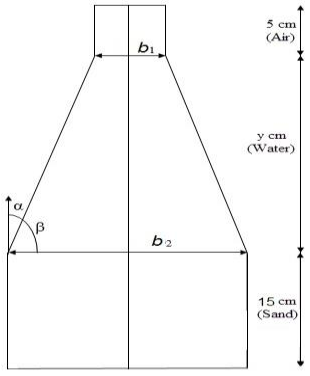

Fig. (5) Side view of side slopes pier with lenticular.

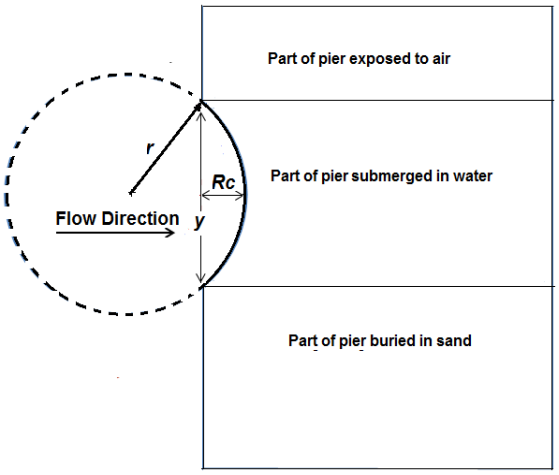

Fig. (6) Elevation of pier Type (C).

6 Procedures of Experiments

To carry out this research, three sets were used. **The first set** includes modified pier with side slope and upstream curved face, side slopes pier with lenticular nose and side slope pier with lenticular nose and upstream curved face were compared. The value of side slope angle α in this comparison is 10°. Also, arc height *Rc* = 3 cm were used in this comparison for modified pier with side slope and upstream curved face, and side slope pier with lenticular nose and upstream curved face. **The second set** included three side slopes piers with lenticular nose has angle α = 0°, 5.71°, and 10°. The side slope angle α = 10° shows the best results as will be presented in the following section, so **the third set** used side slope piers with lenticular nose and upstream curved face have α = 10° and three arc height *Rc* = 1 cm, 2 cm, and 3 cm. The depths of water and tests duration were kept constant and equaled to 10 cm and four hours respectively.

Sand used in this study is non-uniform, so the critical velocity and critical shear velocity were found using formula suggested by Melville and Coleman (2000), and cited in [15].

The used formulae are presented as:

$$V_{ca}^{*} = 0.0115 + 0.012\, d_{50a}^{1.4}\ ,\ 0.1\text{ mm} < d_{50a} < 1\text{mm} \quad (11)$$

$$V_{ca}^{*} = 0.0305\sqrt{d_{50a}} - \frac{0.0065}{d_{50a}}\ ,\ 1\text{mm} < d_{50a} < 100\text{ mm} \quad (12)$$

$$d_{50a} = \frac{d_{max}}{1.8} \quad (13)$$

$$\frac{V_{ca}}{V_{ca}^{*}} = 5.75\ \log\left(5.53\frac{y}{d_{50a}}\right) \quad (14)$$

$$V_a = 0.8\, V_{ca} \quad (15)$$

Where, V_{ca}^{*} is critical shear stress, d_{50a} median size of armor, d_{max} is maximum size of sand particles, V_a is critical average velocity used to clarify the transition from clear water condition to live bed condition for non-uniform sediment flow transport, V_{ca} is average velocity of approach flow. Armoring of non-uniform sand beyond the value of V_a is impossible.

The axis used to display scour hole are illustrated in Fig. (7). These axes is presented as *x* axis at center line of pier and flume and *y* axis located at pier nose where maximum depth of scour is located.

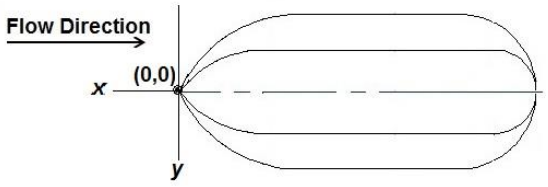

Fig. (7). Locations of *x*, and *y* axes through pier nose.

7 Results Analysis and Discussion

7.1 First Set

This set is used for comparison purposes. Details of this set are displayed in table (1).

TABLE 1
Details of first set

Type of pier	*b1* (cm)	*b2* (cm)	*b* (cm)	*α°*	*y* (cm)
Pier with side slope and upstream curved face. **pier type (A)**	6.5	2.97	4.74	10	10
Side slopes pier with lenticular nose. **pier type (B)**	6.5	2.97	4.74	10	10
Side slope pier with lenticular nose and upstream curved face. **Pier type (C)**	6.5	2.97	4.74	10	10

Three values of Froude number equal 0.26, 0.331 and 0.356 are used in this study related to discharge values equal 19.0273 *lit./s*, 24.28 *lit./s*, and 26.124 *lit./s* respectively. Local scour at pier nose through x axis and y axis are illustrated from Fig. (8) to Fig.(13).

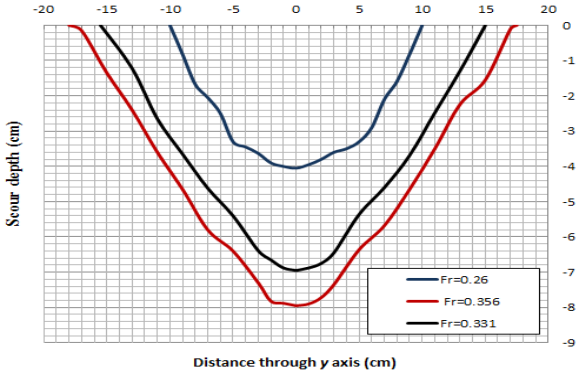

Fig. (8) Scour depth along transverse *y* axis for pier type A.

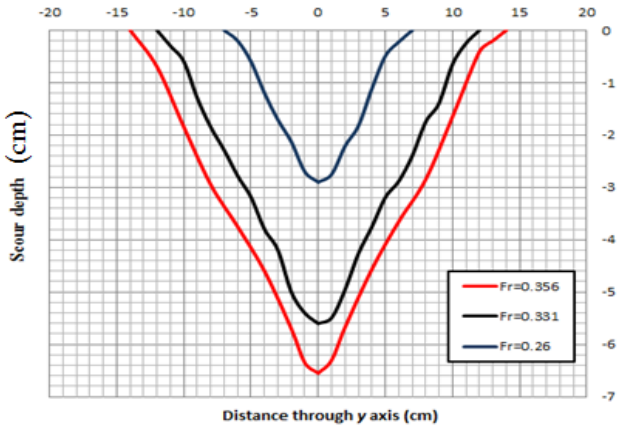

Fig. (9) Scour depth along transverse *y* axis for pier type B.

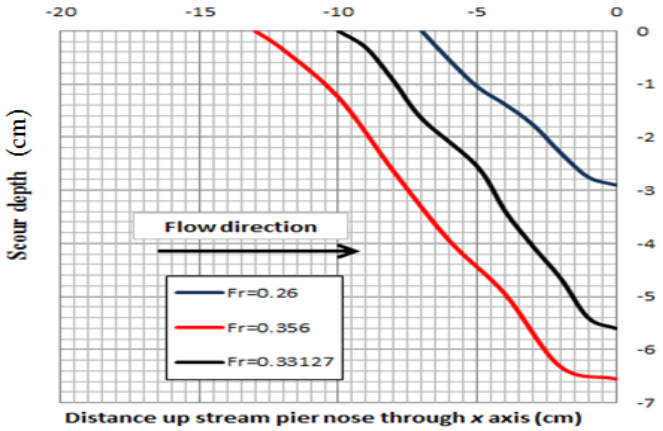

Fig. (12) Scour depth along upstream pier nose through x axis for pier type B.

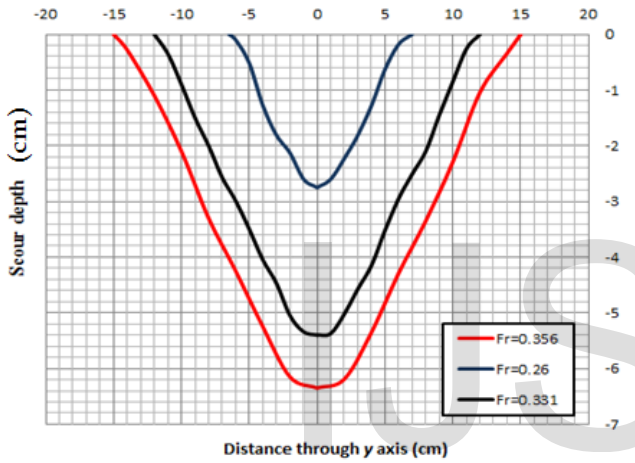

Fig. (10) Scour depth along transverse *y* axis for pier type B.

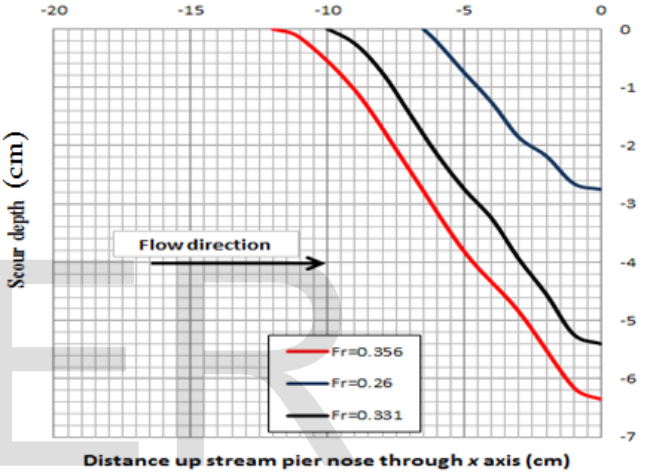

Fig. (13) Scour depth along upstream pier nose through x axis for pier type B.

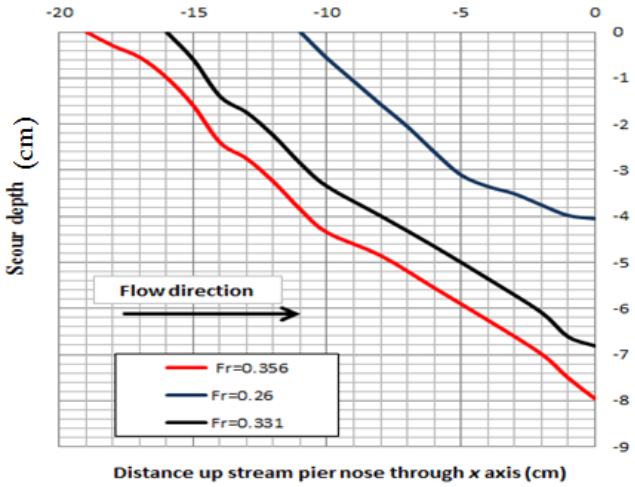

Fig. (11) Scour depth along upstream pier nose through x axis for pier type A.

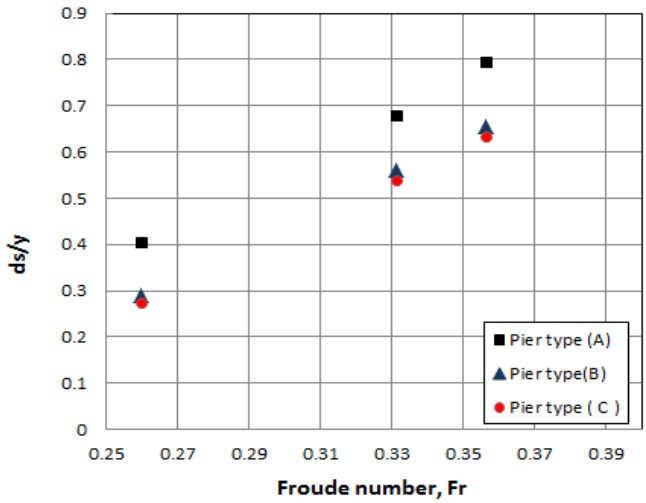

Fig. (14) Variation of dimensionless scour depth (ds/y) versus Froude number for studied pier types.

According to previous figures, maximum scour depth take place at pier nose, and Pier type (C) produced smallest scour depth at pier nose for this study. Also, the width and depth of scour hole for piers Type (B) and (C) are smaller than width

and depth of scour hole for pier type (A). Reduction percent of maximum scour depth for pier type (C) compared with pier type (A) at Fr=0.356 equal 20.13%, while reduction percent of maximum scour depth for pier type (B) compared with pier type (A) at Fr=0.356 equal 17.61%. This reduction on scour depth is occurred because of decreasing the projected area and downward flow component. Lenticular nose and upstream curved face decrease the strength of the vortex system that consists of horseshoe vortex, wake vortex system, and surface roller.

7.2 Second Set: Piers of Type B

The second set includes three side slopes piers with lenticular nose has angle α = 0º, 5.71º, and 10º. Details of data used in this study are clarified in table (2).

TABLE 2
Variables and dimensionless parameters used to develop relations for pier type (B)

Q Lit/s	α^0	β^0	$b2$ (cm)	$b1$ (cm)	b (cm)	y (cm)	ds (cm)	V	ds/y	F_r	V/Va
16.246	0	90	6.5	6.5	6.5	10	3.05	0.21954	0.305	0.221	0.607
16.246	5.71	84.29	6.5	4.5	5.5	10	2.52	0.21954	0.252	0.221	0.607
16.246	10	80	6.5	2.97	4.74	10	2.24	0.21954	0.224	0.221	0.607
19.0273	0	90	6.5	6.5	6.5	10	4.16	0.25713	0.416	0.26	0.711
19.0273	5.71	84.29	6.5	4.5	5.5	10	3.39	0.25713	0.339	0.26	0.711
19.0273	10	80	6.5	2.97	4.74	10	2.9	0.25713	0.29	0.26	0.711
22.482	0	90	6.5	6.5	6.5	10	5.95	0.30381	0.595	0.307	0.84
22.482	5.71	84.29	6.5	4.5	5.5	10	5.25	0.30381	0.525	0.307	0.84
22.482	10	80	6.5	2.97	4.74	10	4.82	0.30381	0.482	0.307	0.84
24.28	0	90	6.5	6.5	6.5	10	6.72	0.32811	0.672	0.331	0.907
24.28	5.71	84.29	6.5	4.5	5.5	10	5.96	0.32811	0.596	0.331	0.907
24.28	10	80	6.5	2.97	4.74	10	5.6	0.32811	0.56	0.331	0.907
26.124	0	90	6.5	6.5	6.5	10	7.76	0.353	0.776	0.356	0.976
26.124	5.71	84.29	6.5	4.5	5.5	10	6.95	0.353	0.695	0.356	0.976
26.124	10	80	6.5	2.97	4.74	10	6.55	0.353	0.655	0.356	0.976

The relation between dimensionless scour depth (*ds/y*) and side slope angle α for this set is displayed in Fig. (15). According to this figure, the maximum scour depth at pier nose decrease with increase in side slope angle α. This reduction in scour depth is due to reduction in projected area and downward flow component.

Fig.(16) clarifies that maximum scour depth increased with increase of Froude number. Also, maximum scour depth increased with increase in flow intensity (*V /Va)* as clarify in Fig. (17). Increase in maximum scour depth with both of *Fr* and (*V /Va)* is related to increase in velocity of flow.

Using dimensional analysis and nonlinear regression program SPSS, two relations of dimensionless scour depth (*ds/y)* relative to Froude number (*Fr*) and flow intensity ($\frac{V}{Va}$) can be obtained separately.

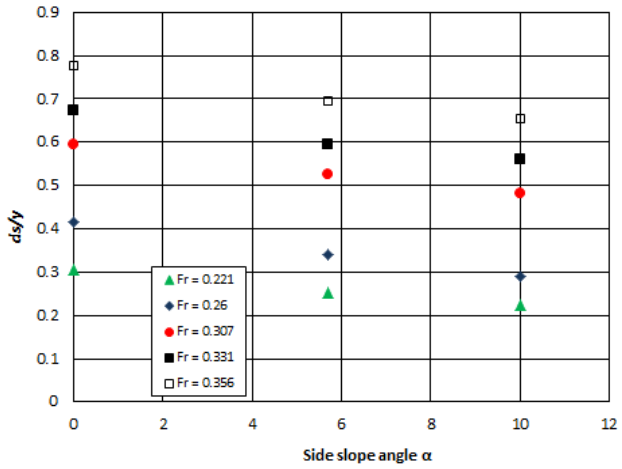

Fig. (15) Variation of *ds/y* versus side slope angle α for different Froude number.

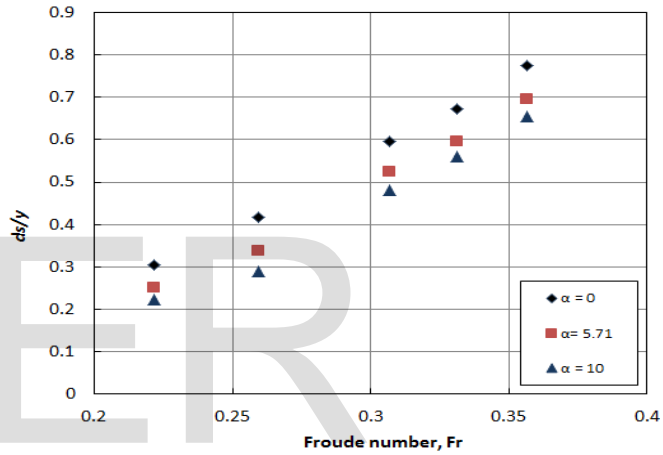

Fig. (16) Variation of ds/y versus Froude number for different side slope angle α.

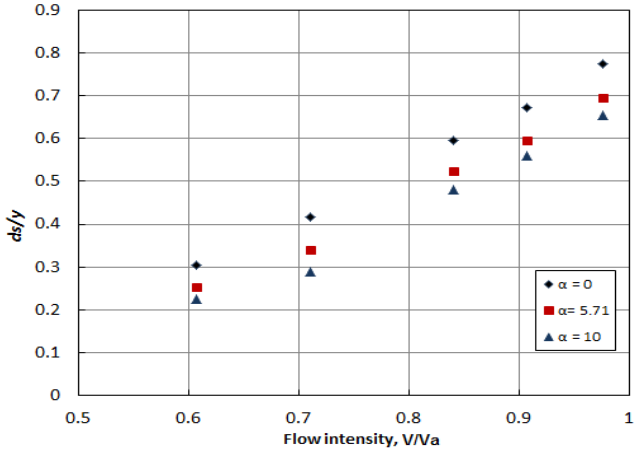

Fig. (17) Variation of *ds/y* versus flow intensity *V /Va* for different side slope angle α.

In nonlinear regression, angle β clarified in Fig. (5) replace angle α in Eq.(5) to avoid the value of α=0. The angle β displayed in table 2. equal to ($90^0 - \alpha$) and it is inserted in radians. Therefore, Eq. (5) can be expressed as:

$$\frac{d_s}{y} = f\left(\frac{V}{V_a}, \frac{V}{\sqrt{gy}}, \beta\right) \quad (16)$$

Influence of Froude number (*Fr*) and flow intensity (*V/Va*) on (*ds/y*) is tested separately with different side slope angle as previously adopted in previous studies, [4], and [5]. Therefore, Eq. (13) can be expressed as follows:

$$\frac{d_s}{y} = f(Fr, \beta) \quad (17)$$

$$\frac{d_s}{y} = f\left(\frac{V}{V_a}, \beta\right) \quad (18)$$

Using nonlinear regression in program SPSS, The relation in Eq.(17) and Eq. (18) can be written as:

$$\frac{d_s}{y} = 3.223 Fr^{2.135} \beta^{1.772} \quad (19)$$

$$\frac{d_s}{y} = 0.375 \left(\frac{V}{V_a}\right)^{2.13} \beta^{1.772} \quad (20)$$

Comparison between measured values (*ds/y*) and computed values of (*ds/y*) using Eq. (19) and Eq. (20) for pier type (B) show good agreement as clarified in Fig. (18) and Fig. (19). Statistical performance indicators used to test precision of these relations are clarified in table (3). Statistical indicators indicate precision of Eq. (19) and Eq. (20) in calculation of maximum scour at pier nose for pier type (B).

TABLE 3
Performance indicators of dimensionless scour depth relations for pier type (B)

Dimensionless scour depth relation	R^2	MAE	RMSE	MAPE
(19)	0.991444	0.013625	0.116726	3.346449
(20)	0.991441	0.014037	0.118479	3.446461

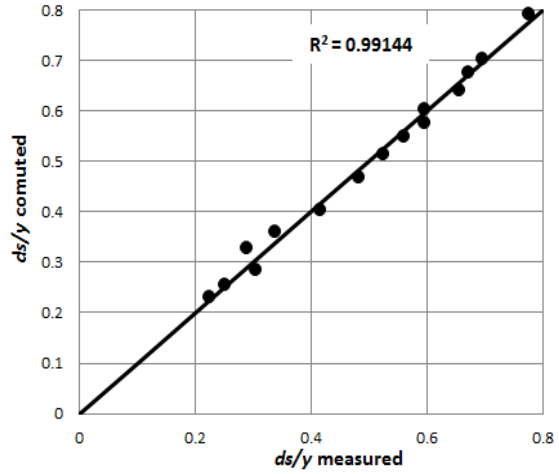

Fig. (18) Comparison between measured *ds/y* and computed *ds/y* using equation (19) for pier type (B).

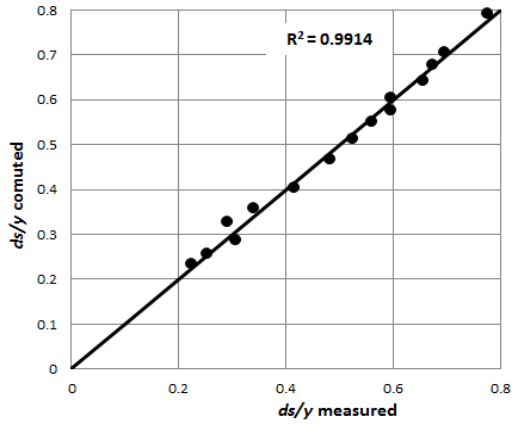

Fig. (19) Comparison between measured *ds/y* and computed *ds/y* using equation (20) for pier type (B).

7.3 Third Set: Piers of Type C

Side slope in third set is kept constant with angle α = 10°. This set of type (C) includes three piers with (*Rc/y*) = 0.1, 0.2, and 0.3. Details of data used in this set are clarified in table (4).

The relation between dimensionless scour depth (*ds/y*) and dimensionless arc height (*Rc/y*) for this set is displayed in Fig. (20). This figure clarifies that maximum scour depth at pier nose decrease with increase in dimensionless arc height (*Rc/y*). This reduction in scour depth is due to reduction in projected area and downward flow component which cause erosion. The reduction of downward flow component for this pier type is more than that for pier type (B) due to the curvature in upstream face of pier. Also, frequency and power of prevailing frequency of vortex shedding decreased with increase of piers side slopes.

Fig. (21) clarifies that maximum scour depth increased with increase of Froude number. Also, maximum scour depth increased with increase in flow intensity (*V /Va)* as clarify in Fig. (22). Increase in maximum scour depth with both of *Fr* and (*V /Va)* is related to increase in velocity of flow.

TABLE 4
Variables and dimensionless parameters used to develop relations for pier type (C)

Q Lit/s	*b2* (cm)	*b1* (cm)	*b* (cm)	*Rc* (cm)	*y* (cm)	*ds* (cm)	*V*	ds/y	F_r	*V/Va*	R_c /y
16.246	6.5	2.97	4.74	1	10	3.2	0.21954	0.32	0.221	0.607	0.1
16.246	6.5	2.97	4.74	2	10	2.67	0.21954	0.267	0.221	0.607	0.2
16.246	6.5	2.97	4.74	3	10	2.13	0.21954	0.213	0.221	0.607	0.3
19.0273	6.5	2.97	4.74	1	10	3.84	0.25713	0.384	0.26	0.711	0.1
19.0273	6.5	2.97	4.74	2	10	3.31	0.25713	0.331	0.26	0.711	0.2
19.0273	6.5	2.97	4.74	3	10	2.75	0.25713	0.275	0.26	0.711	0.3
22.482	6.5	2.97	4.74	1	10	5.98	0.30381	0.598	0.307	0.84	0.1
22.482	6.5	2.97	4.74	2	10	5.29	0.30381	0.529	0.307	0.84	0.2
22.482	6.5	2.97	4.74	3	10	4.6	0.30381	0.46	0.307	0.84	0.3
24.28	6.5	2.97	4.74	1	10	6.74	0.32811	0.674	0.331	0.907	0.1
24.28	6.5	2.97	4.74	2	10	6.02	0.32811	0.602	0.331	0.907	0.2
24.28	6.5	2.97	4.74	3	10	5.4	0.32811	0.54	0.331	0.907	0.3
26.124	6.5	2.97	4.74	1	10	7.71	0.353	0.771	0.356	0.976	0.1
26.124	6.5	2.97	4.74	2	10	6.99	0.353	0.699	0.356	0.976	0.2
26.124	6.5	2.97	4.74	3	10	6.35	0.353	0.635	0.356	0.976	0.3

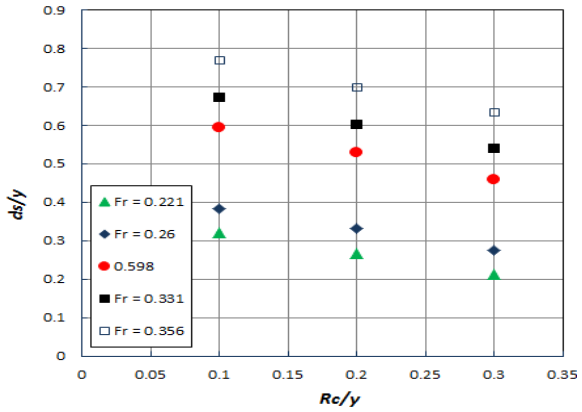

Fig. (20) Variation of *ds/y* versus *Rc/y* for different Froude number.

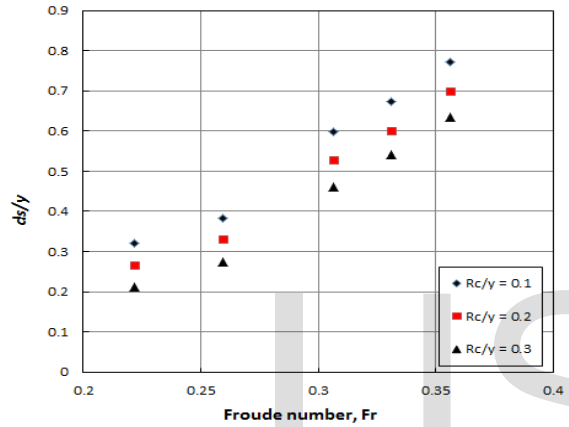

Fig. (21) Variation of *ds/y* versus Froude number for different dimensionless arc height *Rc/y*.

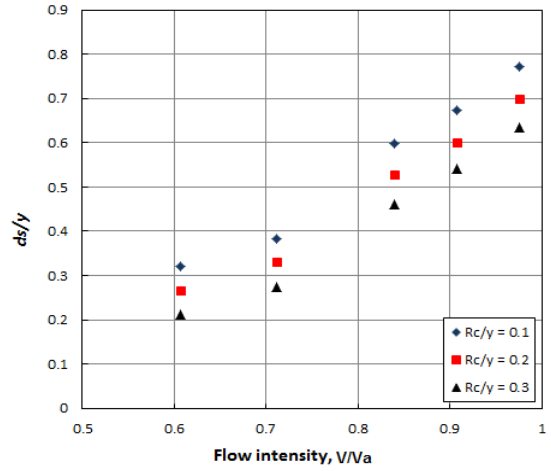

Fig. (22) Variation of *ds/y* versus flow intensity *V/Va* for different dimensionless arc height *Rc/y*.

Using nonlinear regression in program SPSS, The relation in Eq.(6) can be written related to Froude number (*Fr*) and flow intensity (*V/Va*) as:

$$\frac{d_s}{y} = 4.528 Fr^{2.148} (Rc/y)^{-0.208} \qquad (21)$$

$$\frac{d_s}{y} = 0.52 \left(\frac{V}{Va}\right)^{2.143} (Rc/y)^{-0.208} \qquad (22)$$

Comparison between measured values (*ds/y*) and computed values of (*ds/y*) using Eq. (21) and Eq. (22) for pier type (C) show good agreement as clarified in Fig. (23) and Fig. (24) respectively. Statistical performance indicators used to test precision of these relations are clarified in table (5). Statistical indicators indicate precision of Eq. (21) and Eq. (22) in calculation of maximum scour at pier nose for pier type (C).

TABLE 5
Performance indicators of dimensionless scour depth relations for pier type (C)

Dimensionless scour depth relation	R^2	MAE	RMSE	MAPE
(21)	0.9844	0.017425	0.132004	4.685
(22)	0.9849	0.017256	0.131362	4.618877

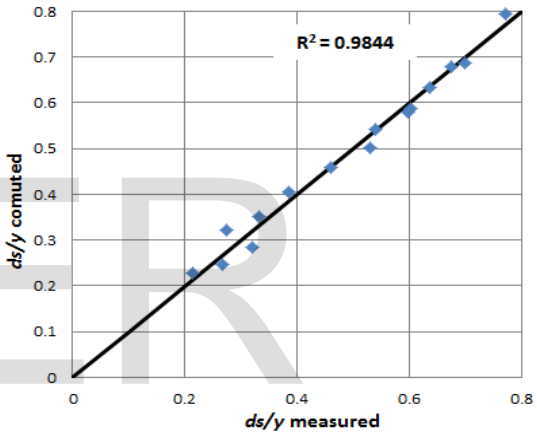

Fig. (23) Comparison between measured *ds/y* and computed *ds/y* using equation (21) for pier type (C).

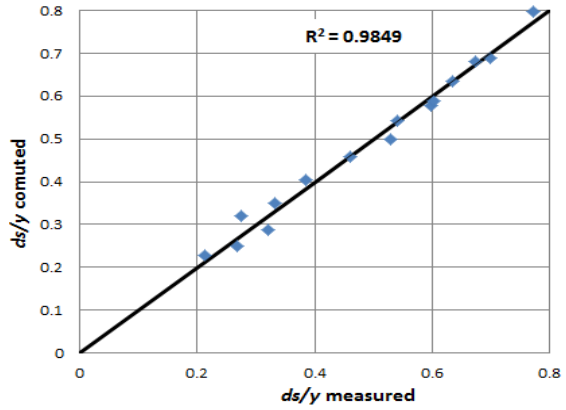

Fig. (24) Comparison between measured *ds/y* and computed *ds/y* using equation (22) for pier type (C).

8 Conclusion

Stability of bridge pier is very for design of bridges crossing watercourses. Side slopes piers with lenticular nose (piers type B) and side slopes piers with lenticular nose modified with upstream curved face (piers type C) were used in this research. These types of piers reduce the projected area, power of wake vortex and influence of downward flow jet at nose of pier which directed to sand bed causing erosion. Empirical relations are developed for the studied two types of piers to guess maximum scour depth at pier's nose. The study was carried out for Froude number range between 0.221 and 0.356, and non-uniform sand bed with d_{50} = 0.63mm under clear water condition. Increase in maximum scour depth occurred with increasing Froude number and flow intensity for the studied two types of piers. Maximum scour depth decreased for piers type (B) with increasing of side slope angle α. Also, maximum scour depth for pier type (c) decreased with increase of dimensionless arc height. The values of maximum scour depth calculated using the proposed relations revealed good agreement compared with measured values.

Notation

In this paper, the following symbols have been used:

b= Mean width of pier;

b_1 = pier width at water surface level;

b_2 = pier width at sand bed;

B = Flume width;

d_{50} = Median particle size;

d_{50a} =Median sediment size for the possible coarsest armor;

d_{max}= Maximum particle size;

ds =Maximum scour depth at pier nose;

y =Approach flow depth;

l = Pier length;

Q= Discharge of flow;

V= Average velocity;

V_a= Critical Average velocity for non-uniform sediment;

V_{ca}= Average velocity of approach flow beyond which the armoring of non-uniform bed is not possible;

V_c= Critical Average velocity of approach for uniform sediment;

Shf = Parameters describing pier shape;

T= Time;

ρ = Fluid density;

ρ_s= Sediment density;

g = Gravity of acceleration;

α = Side slope angle of semi-conical pier;

β = 90- α;

σ_g= Geometric standard deviation;

υ = Kinematic water viscosity;

V_{ca}^*= Critical shear velocity;

Rc=Arc height.

References

[1] Aghaee-Shalmani, Y. and Hakimzadeh H., "Experimental investigation of scour around semi-conical piers under steady current action," *European Journal of Environmental and Civil Engineering*, vol.19, no.6, pp. pp. 717–732, Oct. 2014.

[2] Al-shukur, A.K. and Obied, Z.H., "Experimental study of bridge pier shape to minimize local scour," *International Journal of Civil Engineering and Technology,* vol. 7, no. 1, pp. 162-171, Jan-Feb. 2016.

[3] Alabi, P.D., "Time Development of Local Scour at A Bridge Pier Fitted with A Collar," MSc dissertation, Dept. of Civil and Geological Eng., Saskatchewan University, 2006.

[4] Bozkus, Z. and Yildiz, O., "Effects of inclination of bridge piers on scouring depth," *Journal of Hydraulic Engineering,* vol. 130, No. 8, pp. 827-832, Aug. 2004.

[5] Bozkus, Z. and Cesme M., "Reduction of scouring depth by using inclined piers," *J. Civ. Eng*., vol. 37, pp. 1621-1630, available at http://users.metu.edu.tr /bozkus/html/Reduction%20of%20scouring%20depth%20by%20using%20inclined%20piers.pdf, Oct. 2010.

[6] El- Alfy, K.S., 'Scour and protection at bridge sites in sandy bed channels under steady and unsteady flow conditions', Civil Engineering research magazine, vol. 28, no. 3.,2006

[7] El-Alfy K.S., Shamaa M.T. and Al-tameemi H.H., "Reducing the local Scour around Bridge Piers by Using Semi-conical Piers," *Mansoura Engineering Journal,* vol. 42, no. 2, pp. 10-19, June 2017.

[8] El-Alfy K.S., Shamaa M.T. and Al-tameemi H.H.," Developing local scour equations for piers with side slopes", International Journal of Scientific & Engineering Research, Volume 10, Issue 11, November-2019, ISSN 2229-5518.

[9] Elkhouly, A.M., Shamaa M.T., Sarhan, T.A., Ezzeldin R. M., " Local Scour Around Bridge Abutment", International Journal of Scientific & Engineering Research, Volume 10, Issue 8, August-2019, ISSN 2229-5518

[10] Ismael A., Gunal M. and Hussein H., "Influence of bridge pier position according to flow direction on scour reduction," *ACSEE*, pp. 12-16, 2013.

[11] Melville, B., "The Physics of Local Scour at Bridge Piers," *Fourth International Conference on Scour and Erosion*, pp. 28-40, 2008.

[12] Mia, M.d. and Nago, H., "Design method of time dependent local scour at a circular bridge pier," Journal Hydraulic Engineering, vol. 129, no. 6, pp. 420-427, May 2003.

[13] Ozalp, M.C., "Experimental Investigation of Local Scour Around Bridge Pier Groups," MSc Dissertation, Dept. of Civil Engineering, Middle East Technical University, 2013.

[14] Raudkivi, A.J., and Ettema, R. (1983, Jan.). Clear-water scour at cylindrical piers. Journal of Hydraulic Engineering. 109, pp. 338-350. Available: http://ascelibrary.org/doi/pdf.

[15] Roy, D. and Matin, M.A., "An assessment of local scour at floodplain and main channel of compound channel section.," Journal of Civil Engineering, vol. 38, no. 1, pp. 39-52, 2010.

[16] Talib, A., Obeid, Z.H., and Hameed, H. K., "New Imperial Equation for Local Scour around Various Bridge Piers Shapes", International Journal of Science and Research (IJSR), Volume 5 Issue 9, pp. 654-658, September 2016

[17] Vijayasree, B. A., Eldho, T. I., Mazumder, B. S. and Ahmad, N., "Influence of bridge pier shape on flow field and scour geometry", International Journal of River BasinManagement, pp. 1-21, October 2017, ISSN: 1571-5124 (Print) 1814-2060.

[18] Yanmaz, A.M. and Altinblek, H.D., "Study of time – dependent local scour around bridge piers," *J. Hydraulic Eng.*, vol. 117, no. 10, pp. 1247-1268, Oct. 1991.